

Barrier Function Overrides For Non-Convex Fixed Wing Flight Control and Self-Driving Cars

Eric Squires *Member, IEEE*, Phillip Odom, Zsolt Kira

Abstract—Reinforcement Learning (RL) has enabled vast performance improvements for robotics systems. To achieve these results though, the agent often must randomly explore the environment, which for safety critical systems presents a significant challenge. Barrier functions can solve this challenge by enabling an override that approximates the RL control input as closely as possible without violating a safety constraint. Unfortunately, this override can be computationally intractable in cases where the dynamics are not convex in the control input or when time is discrete, as is often the case when training RL systems. We therefore consider these cases, developing novel barrier functions for two non-convex systems (fixed wing aircraft and self-driving cars performing lane merging with adaptive cruise control) in discrete time. Although solving for an online and optimal override is in general intractable when the dynamics are nonconvex in the control input, we investigate approximate solutions, finding that these approximations enable performance commensurate with baseline RL methods with zero safety violations. In particular, even without attempting to solve for the optimal override at all, performance is still competitive with baseline RL performance. We discuss the tradeoffs of the approximate override solutions including performance and computational tractability.

I. INTRODUCTION

REINFORCEMENT learning (RL) presents significant deployment challenges for safety critical systems. While the performance can often vastly exceed other approaches, the propensity to unpredictably fail can render its employment impractical. On the other hand, barrier functions [1], [2] excel at enabling safety assurance, but require simplifying assumptions on the system dynamics to compute control inputs that enforce the safety constraint, making it difficult to apply to problems where RL excels. Two examples of this type of problem are waypoint following for fixed wing aircraft and lane merging with adaptive cruise control for self-driving cars, both of which can be non-convex in the control input and therefore make computing a safe control computationally intractable. Nevertheless, after deriving novel barrier functions for these systems we investigate computationally tractable approximations to a barrier function override, finding that this enables both safety assurance and high performance even relative to model free safe RL baselines.

A barrier function is an output function of the system state that enables safety assurance. When used to ensure safety with RL, the RL policy first outputs a nominal control value. Given this control value, a safe control value is computed through an optimization that is as close as possible to the nominal control

Eric Squires and Phillip Odom are with the Georgia Tech Research Institute. Zsolt Kira is with the College of Computing at the Georgia Institute of Technology. Corresponding Author: Eric Squires. 250 14th St, Atlanta, GA, 30318. (email: eric.squires@gtri.gatech.edu; phillip.odom@gtri.gatech.edu; zkira@gatech.edu)

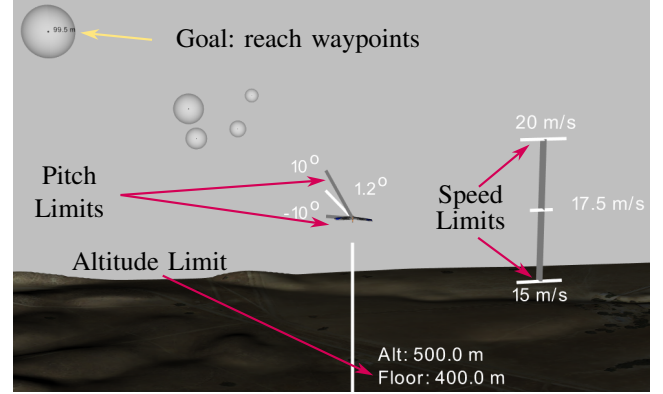


Fig. 1: Screenshot of the UAV environment with safety conditions visualized with SCRIMAGE [3].

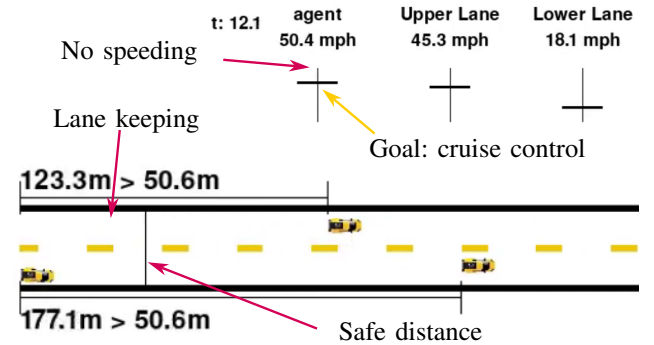


Fig. 2: Screenshot of the car environment with safety conditions.

value without violating the barrier constraint. As shown in [1], under the assumption that the system is linear in the control input, this optimization can be computed efficiently for online overrides.

However, restricting allowable dynamics to those that are linear in the control input may limit the fidelity of system. For instance, air drag is nonlinear in the load factor for aircraft. Similarly, due to transformations between reference frames, trigonometric functions give rise to systems that are non-convex in the control input. A more thorough list of such systems can be found in [4], [5]. At the same time, RL does not make this assumption, meaning that finding a way for barrier functions to be successfully employed in systems that are nonlinear in the control input can broaden their applicability for difficult, safety critical problems.

Aside from being applicable to dynamics that are nonconvex in the control input, RL introduces an additional challenge

because of its discrete time formulation. As shown in [6], when time is discrete, the optimization to compute a safe control input can become non-convex, which cannot in general be solved in real time. This can occur even when the dynamics are linear. One solution is to accept that there is a gap between the theory and implementation by deriving barrier function properties in continuous time and then deploying them in discrete time (e.g. [7], [8]). Unfortunately, this requires the discrete timestep to be small so that the continuous time dynamics and barrier function derivative are reasonable approximations of the discrete step updates. As an example from [9], the simulation had to run at 200 Hz to avoid collisions. Short timesteps make it more difficult for RL algorithms to learn [10] so this can significantly increase training time or impede final performance. Another approach [11] accounts for the discretization errors by including an adjustment to the barrier constraint condition that is the worst case error over the reachable set within one timestep. However, computing this reachable set for nonlinear systems requires conservative approximations to make it computationally efficient.

Given the non-convex optimization in discrete time barrier functions, a variety of solutions have been proposed. In [12], the authors use model predictive control (MPC) to solve an optimization including the barrier function constraint, a Lyapunov constraint, and performance objectives. They show that by using more than the one step horizon the performance can be improved. However, as it is computationally prohibitive to solve a nonlinear MPC problem as the horizon grows, the optimization may be infeasible. Multi-step horizons have been shown elsewhere to either improve performance [13], expand the safe set [14], or construct barrier functions [15]. Recursive feasibility for nonlinear MPC with barrier functions is analyzed in [16] which introduces quasi-barrier functions that can be used to expand the set of feasible states and ensure recursive feasibility. They also apply the result to lane merging although the approach requires a centralized computation involving the other vehicle. Aside from using MPC to address the non-convex optimization, another approach [17] is to find a lower bound to the barrier constraint where the lower bound is linear in the control input. In particular, under the assumption of bounded uncertainty in a collision avoidance task with a lower bound on the constraint, the non-convex optimization [17] transforms into a quadratic program. However, this approach requires exploiting particular details of the multi-agent system.

RL, on the other hand, can excel in environments that are non-convex. While RL can induce unsafe policies, there are a variety of approaches to improve safety characteristics. Nevertheless, while these approaches can yield policies that are more sensitive to safety considerations, safety violations can still occur. In [18], the authors show how to efficiently evaluate surrogate cost and objective functions with bounded errors for a proposed policy based on data from a different policy and incorporate this insight into a trust region optimization. Lagrangian approaches [19] similarly seek to solve a constrained optimization where reward is maximized subject to cost limits. In this approach, a cost coefficient is adaptively updated so that costs stay below an upper bound. This approach was used with barrier functions for instance

in [13] where a learned barrier function constraint is used instead of a discounted cost estimate. Similarly, [20] learns a barrier function that satisfies some of the required properties by design and trains an override policy to be safe with respect to the learned barrier function. To induce exploration, they add noise to this policy and if after resampling there are no safe actions, revert to the certified safe policy. Action masking is also investigated based on cost thresholds in [21] where the override policy is trained to minimize the expected discounted cost. Similarly, [22] also includes a Lagrangian term to induce the nominal policy to include cost considerations. In [23], the authors note that applying overrides that are not significantly safer than the nominal policy can lead to worse performance so they therefore require that the override provide an improvement over a threshold in order to be used. Rather than explicitly computing a safe override policy, [24] computes an online adjustment to actions proposed by a nominal policy. In particular, given a function estimating the discounted cost, they adjust the action using gradient descent to find a safe override. Unfortunately, none of these approaches can assure that the system will stay safe throughout training or be safe at deployment after training is completed.

This paper addresses how to enable safe control overrides using barrier functions for systems that are non-convex in the control input. It makes the following contributions. First, we derive barrier functions for two such systems, namely fixed wing aircraft performing waypoint following subject to safe flight envelope constraints and self driving cars doing lane merging with adaptive cruise control. Second, we develop RL environments for both fixed wing aircraft and self driving cars. Third, we provide an experimental examination of the effect of different safety override approximations on RL performance as well as compare to safe RL baselines. In particular, we find that all of the discussed overrides yield performance commensurate with the highest performing baselines without any safety violations. This holds even when the safety override makes no attempt to match the nominal control value output.

This paper is organized as follows. In Section II, we provide background for barrier functions. In Section III, IV, and V, we derive barrier functions for fixed-wing aircraft, a double integrator, and self-driving cars, respectively. We introduce RL environments to compare a barrier function override for fixed wing aircraft and self-driving cars with simulated experimental results in Section VI. Section VII concludes.

II. BACKGROUND

Background for RL can be found in [25]. Discrete time barrier functions were analyzed in [6]. Let the system have dynamics

$$s_{k+1} = f(s_k, u_k) \quad (1)$$

where $s_k \in \mathbb{R}^{n_s}$ and $u_k \in U \subseteq \mathbb{R}^{n_u}$. An output function $h : \mathbb{R}^{n_s} \rightarrow \mathbb{R}$ with superlevel set

$$C_h = \{s_k : h(s_k) \geq 0\} \quad (2)$$

can be used to ensure the safety of a system. Definition 1 and Proposition 1 are from [26] which rephrases Definition 4 and Proposition 4 of [6] using terminology from [1].

Definition 1. A map $h : \mathbb{R}^{n_s} \rightarrow \mathbb{R}$ is a Discrete-Time Exponential Control Barrier Function (DT-ECBF) on a set $D_h \subseteq \mathbb{R}^{n_u}$ where $C_h \subseteq D_h$ with C_h defined in (2) if for all $s_k \in D_h$ there is a $u_k \in \mathbb{R}^{n_u}$ and $\lambda \in (0, 1]$ such that

$$c_h(s_k, u_k) \triangleq h(f(s_k, u_k)) - (1 - \lambda)h(s_k) \geq 0. \quad (3)$$

The admissible control space is

$$K_h(s_k) = \{u_k \in U : c_h(s_k, u_k) \geq 0\}.$$

Proposition 1. Given a set $C_h \subset \mathbb{R}^{n_s}$ defined in (2) for an output function h , let h be a DT-ECBF on D_h and $u : \mathbb{R}^{n_s} \rightarrow U$ be such that $u(s_k) \in K_h(s_k)$ for all $s_k \in D_h$. Then if $s_0 \in C_h$ then $s_k \in C_h$ for all $k > 0$.

In [1], the authors introduce an optimization that solves for a safe control value that minimizes the squared distance to a nominal control value \hat{u}_k . If h is non-convex, then the following can be non-convex even when the dynamics (1) are linear [6]:

$$\begin{aligned} u_k^* &= \arg \min_{u_k \in \mathbb{R}^{n_u}} \frac{1}{2} \|u_k - \hat{u}_k\|^2 \\ \text{s.t.} \quad & c_h(s_k, u_k) \geq 0 \\ & u_k \in U. \end{aligned} \quad (4)$$

In [15] the authors develop an approach for generating a barrier function given a safety function $\rho : \mathbb{R}^{n_s} \rightarrow \mathbb{R}$ which encodes a safety specification. In [26] this approach is adapted to discrete time systems. Given a safety function ρ and evasive maneuver $\zeta : \mathbb{R}^{n_s} \rightarrow U$, a DT-ECBF can be constructed via

$$h(s_0) = \inf_{k \geq 0} \rho(\hat{s}_k) \quad (5)$$

with $\hat{s}_0 = s_0$ and $\hat{s}_{k+1} = f(\hat{s}_k, \zeta(\hat{s}_k))$.

III. A BARRIER FUNCTION FOR FIXED WING AIRCRAFT

RL for waypoint following has been previously discussed e.g., in [27], although they did not consider safety. Composition of multiple constraints using barrier functions has been developed for fixed wing aircraft for collision avoidance [15] as well as collision avoidance with a geofence constraint [28]. Here though we consider a model from [29] that is non-convex in the control input. The model considers UAV speed, pitch, and heading. Because we examine a waypoint following problem in Section VI we also include position dynamics. The discrete time dynamics of the model in [29] for discrete time is then given by

$$v_{k+1} = v_k + \delta g([T_k - \mathcal{D}(v_k, n_k)]/W - \sin(\gamma_k)) \quad (6a)$$

$$\gamma_{k+1} = \gamma_k + \delta g(n_k \cos(\mu_k) - \cos(\gamma_k))/v_k \quad (6b)$$

$$\psi_{k+1} = \psi_k + \delta g n_k \sin(\mu_k)/(v_k \cos(\gamma_k)) \quad (6c)$$

$$x_{k+1} = x_k + \delta v_k \cos(\gamma_k) \cos(\psi_k) \quad (6d)$$

$$y_{k+1} = y_k + \delta v_k \cos(\gamma_k) \sin(\psi_k) \quad (6e)$$

$$z_{k+1} = z_k + \delta v_k \sin(\gamma_k) \quad (6f)$$

where $\delta > 0$ is a timestep, g is gravity, $(v_k, \gamma_k, \psi_k)^T$ are speed, pitch, and heading while $(x_k, y_k, z_k)^T$ are positions. The state

is then $s_k = (v_k, \gamma_k, \psi_k, x_k, y_k, z_k)^T$ while the control input $u_k = (T_k, n_k, \mu_k)^T$ consists of the thrust, load factor, and bank angle where load factor is the ratio of weight to lift force. The control input u_k is subject to actuator constraints

$$U = \{u \in \mathbb{R}^{n_u} : T_k \in [0, T_{max}], n_k \in [n_{min}, n_{max}], \mu_k \in [-\mu_{max}, \mu_{max}]\}. \quad (7)$$

Finally,

$$\mathcal{D}(v_k, n_k) = 0.5 \mathcal{R} v_k^2 A C_{D0} + 2 \mathcal{K} n_k^2 W^2 / (\mathcal{R} v_k^2 A) \quad (8)$$

is the drag force where \mathcal{R} is the air density, A is the wing surface area, C_{D0} is the parasitic drag coefficient, \mathcal{K} is the induced drag coefficient, and W is the weight of the vehicle. This model is nonlinear in n_k and non-convex in μ_k .

The safety condition encompasses stall conditions, excessive speed that can stress the aircraft platform, and maintaining an altitude above a floor z_{min} . Given $v_{min} > 0$, let

$$S = \{s_k \in \mathbb{R}^{n_s} : \gamma_k \in [\gamma_{min}, \gamma_{max}], v_k \in [v_{min}, v_{max}], z_k \geq z_{min}\}. \quad (9)$$

Let

$$\alpha(s_k) = \min(\gamma_{max} \lambda v_k / \delta, g n_{max} - g), \quad (10)$$

$$\tilde{n}(s_k) = \cos(\gamma_k) + \frac{1}{g} \min\left(\frac{\lambda v_k}{\delta} (\gamma_{max} - \gamma_k), \alpha(s_k)\right) \quad (11)$$

$$\tilde{T}(s_k) = W \sin(\gamma_k) + \mathcal{D}(v_k, \tilde{n}(s_k)) \quad (12)$$

$$\tilde{\mu}(s_k) = 0 \quad (13)$$

$$\tilde{u}(s_k) = (\tilde{T}(s_k), \tilde{n}(s_k), \tilde{\mu}(s_k))^T \quad (14)$$

$$\tau(s_k) = -\gamma_k / (\alpha(s_k) / v_k) \quad (15)$$

Denote $\alpha_k = \alpha(s_k)$, $\tilde{T}_k = \tilde{T}(s_k)$, $\tilde{n}_k = \tilde{n}(s_k)$, $\tilde{\mu}_k = \tilde{\mu}(s_k)$, $\tilde{u}_k = \tilde{u}(s_k)$, and $\tau_k = \tau(s_k)$. For some intuition on α and τ , note that if pitch is negative, i.e. $\gamma_k < 0$, then the load factor $\tilde{n}(s_k) = \cos(\gamma_k) + \alpha(s_k)/g$ in (11). Then $\gamma_{k+1} - \gamma_k = \delta \alpha(s_k) / v_k$ in (6b) so that $\alpha(s_k) / v_k$ can be interpreted as the change in pitch per unit time. Noting that $v_{k+1} = v_k$ in (6a) given \tilde{T} in (12) so $\alpha(s_k)$ is constant, we can then interpret τ as the time to reach zero pitch.

Let

$$b_1(s_k) = v_{max} - v_k \quad (16a)$$

$$b_2(s_k) = v_k - v_{min} \quad (16b)$$

$$b_3(s_k) = \gamma_{max} - \gamma_k \quad (16c)$$

$$b_4(s_k) = \gamma_k - \gamma_{min} \quad (16d)$$

$$b_5(s_k) = z_k + v_k \min(0, \gamma_k)(\max(\tau_k, 0) + \delta) - z_{min} \quad (16e)$$

We then define a candidate barrier function

$$h_{fw}(s_k) = \min_{i \in \{1, \dots, 5\}} b_i(s_k). \quad (17)$$

The following can be computed with a straightforward application of derivatives to (8) and (12):

$$\tilde{T}_{max} = \max_{x \in \mathbb{R}^{n_s} : v_k \in [v_{min}, v_{max}], \gamma_k \in [\gamma_{min}, \gamma_{max}]} \tilde{T}(s_k) \quad (18)$$

$$\tilde{T}_{min} = \min_{x \in \mathbb{R}^{n_s} : v_k \in [v_{min}, v_{max}], \gamma_k \in [\gamma_{min}, \gamma_{max}]} \tilde{T}(s_k) \quad (19)$$

For the candidate h_{fw} to be useful for keeping the system safe, we must have $C_{h_{fw}} \subseteq S$ where $C_{h_{fw}}$ is defined in (2) using h_{fw} . Hence we first show conditions under which $b_i(s_k) \geq 0$ for $i = 1, \dots, 5$ implies $s_k \in S$. We then show when $\tilde{u}_k \in U$ and $b_i(f(s_k, \tilde{u}_k)) + (1 - \lambda)b_i(s_k) \geq 0$ for $i = 1, \dots, 5$. Finally, we give sufficient conditions under which a minimum of functions is a barrier function so that h_{fw} in (17) is a barrier function.

Lemma 1. Suppose $v_{min} > 0$, $n_{max} > 1$, $\gamma_{max} > 0$, and $b_2(s_k) \geq 0$. Then $\alpha_k > 0$.

Proof. This holds by direct substitution into (10). \square

Theorem 1. Let the assumptions of Lemma 1 hold. For $s_k \in \mathbb{R}^{n_s}$, if $b_i(s_k) \geq 0$ for $i = 1, \dots, 5$ defined in (16), $s_k \in S$ where S is defined in (9).

Proof. From the definition of b_i for $i = 1, \dots, 4$, $\gamma_k \in [\gamma_{min}, \gamma_{max}]$ and $v_k \in [v_{min}, v_{max}]$ so $v_k \geq v_{min} > 0$. We now show that $z_k \geq z_{min}$. If $\gamma_k < 0$ then because $\alpha_k > 0$ by Lemma 1, $\tau_k > 0$. Then $0 \leq b_5(s_k) = z_k + v_k\gamma_k(\tau_k + \delta) - z_{min} \leq z_k - z_{min}$. If $\gamma_k \geq 0$ then $0 \leq b_5(s_k) = z_k - z_{min}$. Then $s_k \in S$. \square

Lemma 2. Let the assumptions of Lemma 1 hold. Let \tilde{T}_{min} and \tilde{T}_{max} be defined in (18) and (19), respectively, and suppose $0 \leq \tilde{T}_{min}$, $\tilde{T}_{max} \leq T_{max}$, and $n_{min} \leq \min(\cos(\gamma_{min}), \cos(\gamma_{max}))$. If $s_k \in \mathbb{R}^k$ satisfies $b_i(s_k) \geq 0$ for $i \in \{1, \dots, 4\}$ then for \tilde{u} and U defined in (14) and (7), respectively, $\tilde{u}(s_k) \in U$.

Proof. From (13), $\tilde{\mu}_k = 0 \in [-\mu_{max}, \mu_{max}]$ and by assumption $\tilde{T}_k \in [0, T_{max}]$. By Lemma 1, $\alpha_k > 0$. By assumption $b_3(s_k) \geq 0$ and $b_4(s_k) \geq 0$ so $\gamma_k \in [-\gamma_{min}, \gamma_{max}]$. Then from (11) we have $\tilde{n}_k \geq \cos(\gamma_k) \geq \min(\cos(\gamma_{min}), \cos(\gamma_{max})) \geq n_{min}$. Similarly, from (10) and (11), $\tilde{n}_k \leq \cos(\gamma_k) + \alpha_k/g \leq \cos(\gamma_k) + (gn_{max} - g)/g = \cos(\gamma_k) + n_{max} - 1 \leq n_{max}$. \square

Lemma 3. Let the assumptions of Lemma 2 hold. For the system (6), if $b_i(s_k) \geq 0$ for $i = 1, \dots, 5$ in (16) where $s_k \in \mathbb{R}^{n_s}$ then for $i = 1, \dots, 5$

$$b_i(f(s_k, \tilde{u}(s_k))) - (1 - \lambda)b_i(s_k) \geq 0. \quad (20)$$

where $\tilde{u}(s_k)$ is defined in (14).

Proof. Denote $\tilde{u}_k \triangleq \tilde{u}(s_k)$ which is in U by Lemma 2. Given \tilde{u}_k , $v_{k+1} = v_k$ so (20) is satisfied for $i = 1, 2$. Since from Lemma 1 we have $\alpha_k > 0$ and the assumption $b_3(s_k) \geq 0$ implies $\gamma_k \leq \gamma_{max}$, we have $\tilde{n}_k \geq \cos(\gamma_k)$ which implies $\gamma_{k+1} \geq \gamma_k$ so (20) is satisfied for $i = 4$. For $i = 3$ and again given \tilde{u}_k in (14), $\gamma_{k+1} \leq \gamma_k + \lambda(\gamma_{max} - \gamma_k)$, so that

$$\begin{aligned} & b_3(f(s_k, \tilde{u}_k)) - (1 - \lambda)b_3(s_k) \\ & \geq \gamma_{max} - (\gamma_k + \lambda(\gamma_{max} - \gamma_k)) - (1 - \lambda)(\gamma_{max} - \gamma_k) \\ & = 0. \end{aligned}$$

We now show (20) holds for $i = 5$. Suppose $0 \leq \gamma_k \leq \gamma_{max}$. Then because $v_k \geq v_{min} > 0$, $z_{k+1} \geq z_k$. Further, since $\alpha_k > 0$ from Lemma 1, we have $\tilde{n}_k > \cos(\gamma_k)$ so $\gamma_{k+1} \geq \gamma_k \geq 0$. Then $b_5(f(s_k, \tilde{u}_k)) = z_{k+1} - z_{min} \geq z_k - z_{min} \geq b_5(s_k)$ so (20) holds for this case.

Consider then $\gamma_{min} \leq \gamma_k < 0$. In this case we have $\alpha_k \leq \lambda v_k(\gamma_{max} - \gamma_k)/\delta$ so $\tilde{n}_k = \cos(\gamma_k) + \alpha_k/g$ which implies that $\gamma_{k+1} = \gamma_k + \delta\alpha_k/v_k$. Also note $\alpha_k > 0$ from Lemma 1.

If $\gamma_k \leq -\delta\alpha_k/v_k$ then $\tau_k \geq \delta$, $\tau_{k+1} = -\gamma_{k+1}/(\alpha_k/v_k) = -(\gamma_k + \delta\alpha_k/v_k)/(\alpha_k/v_k) = \tau_k - \delta$, and $b_5(s_k) = z_k + v_k\gamma_k(\tau_k + \delta) - z_{min}$. Recall that for \tilde{u}_k we have $v_{k+1} = v_k$, from Lemma 1 that $\alpha_k > 0$, and note that since $\gamma_k < 0$ we have $\sin \gamma_k > \gamma_k$. Then

$$\begin{aligned} & b_5(f(s_k, \tilde{u}_k)) \\ & = z_k + \delta v_k \sin \gamma_k + v_k(\gamma_k + \delta\alpha_k/v_k)(\tau_k - \delta + \delta) - z_{min} \\ & \geq z_k + \delta v_k \gamma_k + v_k \gamma_k \tau_k - z_{min} \\ & = b_5(s_k). \end{aligned}$$

For $-\delta\alpha_k/v_k < \gamma_k < 0$, we have $0 < \tau_k < \delta$. Further, $\gamma_{k+1} = \gamma_k + \delta\alpha_k/v_k \geq -\delta\alpha_k/v_k + \delta\alpha_k/v_k = 0$ so $\tau_{k+1} \leq 0$. Then

$$\begin{aligned} & b_5(f(s_k, \tilde{u}_k)) = z_k + \delta v_k \sin \gamma_k - z_{min} \\ & \geq z_k + \delta v_k \gamma_k - z_{min} \\ & \geq z_k + (\delta + \tau_k)v_k \gamma_k - z_{min} \\ & = b_5(s_k). \end{aligned}$$

\square

Barrier function composition has been previously discussed for continuous time in [30], [31]. In [26], the authors showed that the maximum of barrier functions is a barrier function. For the case of a minimum of barrier functions, we need an additional condition. This extra condition is similar to the shared evasive maneuver assumption discussed in [15].

Lemma 4. Let q_i for $i = 1, 2$ be real valued functions on \mathbb{R}^{n_s} with q_3 defined by $q_3(s_k) = \min_{i=1,2} q_i(s_k)$. Choose $s_k \in \mathbb{R}^{n_s}$ and assume there exists some u_k such that $q_i(f(s_k, u_k)) - (1 - \lambda)q_i(s_k) \geq 0$ for $i = 1, 2$. Then $q_3(f(s_k, u_k)) - (1 - \lambda)q_3(s_k) \geq 0$.

Proof. Without loss of generality assume $q_1(s_k) \leq q_2(s_k)$. If $q_1(f(s_k, u_k)) \leq q_2(f(s_k, u_k))$ then $c_{q_3}(s_k, u_k) = c_{q_1}(s_k, u_k) \geq 0$. If $q_1(f(s_k, u_k)) > q_2(f(s_k, u_k))$ then

$$\begin{aligned} & c_{q_3}(s_k, u_k) = q_2(f(s_k, u_k)) - (1 - \lambda)q_1(s_k) \\ & \geq q_2(f(s_k, u_k)) - (1 - \lambda)q_2(s_k) \\ & = c_{q_2}(s_k, u_k) \geq 0. \end{aligned}$$

\square

Corollary 1. Let h_1 and h_2 be DT-ECBFs on D_1 and D_2 , respectively. Suppose that for any $s_k \in D_1 \cap D_2$ there is a $u_k \in U$ such that $c_{h_1}(s_k, u_k) \geq 0$ and $c_{h_2}(s_k, u_k) \geq 0$. Then h_3 defined by $h_3(s_k) = \min_{i=1,2} h_i(s_k)$ is a DT-ECBF on $D_1 \cap D_2$.

Proof. From Lemma 4, for any $s_k \in D_1 \cap D_2$, there is a $u_k \in U$ such that $c_{h_3}(s_k, u_k) \geq 0$. Then h_3 is a DT-ECBF. \square

Theorem 2. Let the assumptions of Lemma 3 hold. Then h_{fw} in (17) is a DT-ECBF.

Proof. Let $s_k \in \mathbb{R}^{n_s}$ where $h_{fw}(s_k) \geq 0$. Then $b_i(s_k) \geq 0$ for $i = 1, \dots, 5$. Then from Lemma 2, $\tilde{u}_k \in U$ and from Lemma

3, b_i satisfies (20) for $i = 1, \dots, 5$. Then from Lemma 4 and induction, h_{fw} satisfies (3). \square

Remark 1. b_1 and b_2 in (16a)-(16b) are not necessarily barrier functions. For instance, let $v_k = v_{\min}$ and $\pi/2 \geq \gamma_k > \gamma_{\max}$. Then $b_1(s_k) \geq 0$. Suppose $k = C_{D0} = 0$ so that $\mathcal{D}(v_k, n_k) = 0$. If $T_{\max} = W \sin(\gamma_{\max})$, then for any $u_k \in U$, $v_{k+1} \leq v_k + \delta g(T_{\max}/W - \sin(\gamma_k)) = v_k + (\sin(\gamma_{\max}) - \sin(\gamma_k)) < v_{\min}$. A similar calculation shows b_2 is not a barrier function when $v_k = v_{\max}$ and $\gamma_k < -\gamma_{\max}$. Hence we use Lemma 4 rather than Corollary 1 in the proof of Theorem 2.

IV. BARRIER FUNCTION FOR A DOUBLE INTEGRATOR

Barrier functions for continuous time double integrator systems have been previously been analyzed in [32] and [33]. A higher order integrator was analyzed in [34]. Here we derive a barrier function for discrete time where the double integrator dynamics are given by

$$p_{k+1} = p_k + \delta v_k \quad (21a)$$

$$v_{k+1} = v_k + \delta a_k \quad (21b)$$

where the state $s_k = (p_k, v_k)^T$ consists of position and velocity while the input $a_k \in [a_{\min}, a_{\max}]$ is the acceleration.

Although this double integrator is linear in the control input, we use the results in this section for the non-convex self-driving car system in the next section. The floor function is denoted by $\lfloor \cdot \rfloor$. For $\tilde{a} = (a^-, a^+)^T \in \mathbb{R}^2$ with $a^- \in [a_{\min}, 0)$ and $a^+ \in (0, a_{\max}]$, let

$$\tilde{u}_{dbl}(s_k, \tilde{a}) = \begin{cases} \max(a^-, -v_k/\delta) & v_k \geq 0 \\ \min(a^+, -v_k/\delta) & v_k < 0 \end{cases} \quad (22)$$

$$A(s_k, \tilde{a}) = \begin{cases} a^- & v_k \geq 0 \\ a^+ & v_k < 0 \end{cases} \quad (23)$$

$$N(s_k, \tilde{a}) = \lfloor |v_k| / |\delta A(s_k, \tilde{a})| \rfloor \quad (24)$$

$$\eta(s_k, \tilde{a}) = p_k + \delta N(s_k, \tilde{a}) v_k + \frac{N(s_k, \tilde{a})(N(s_k, \tilde{a}) - 1)}{2} \delta^2 A(s_k, \tilde{a}) + \delta(v_k + \delta N(s_k, \tilde{a}) A(s_k, \tilde{a})) \quad (25)$$

Lemma 5. For a system with dynamics (21), suppose for all integers $l \geq 0$ that $a_{k+l} = \tilde{u}_{dbl}(s_{k+l}, \tilde{a})$ for $\tilde{a} = (a^-, a^+)^T \in \mathbb{R}^2$ with $a^- \in [a_{\min}, 0)$ and $a^+ \in (0, a_{\max}]$. Then

- a) $p_{k+l} = \eta(s_k, \tilde{a})$ for all $l > N(s_k, \tilde{a})$.
- b) If $v_k \geq 0$ then $p_{k+l} \leq \eta(s_k, \tilde{a})$ for all $l \geq 0$. If $v_k \leq 0$ then $p_{k+l} \geq \eta(s_k, \tilde{a})$ for all $l \geq 0$.
- c) η is continuous in s_k and $\eta(s_k, \tilde{a}) = \eta(f(s_k, \tilde{u}_{dbl}(s_k, \tilde{a})), \tilde{a})$.
- d) η increases as v_k increases.

Proof. Consider the case where $v_k \geq 0$ as the other case follows similarly. We first show that for nonnegative integers l

$$v_{k+l} = \begin{cases} v_k + l\delta a^- & l \leq N(s_k, \tilde{a}) \\ 0 & l > N(s_k, \tilde{a}) \end{cases} \quad (26)$$

This holds trivially for $l = 0$. Suppose it holds for some l satisfying $0 \leq l \leq N(s_k, \tilde{a}) - 1$. Then from (24), $v_k \geq$

$N(s_k, \tilde{a})\delta|a^-| \geq (l+1)\delta|a^-| = -(l+1)\delta a^-$. Then from the induction hypothesis, $v_{k+l} = v_k + l\delta a^- \geq -(l+1)\delta a^- + l\delta a^- = -\delta a^-$ so $-v_{k+l}/\delta \leq a^-$ and $\tilde{u}_{dbl}(s_{k+l}, \tilde{a}) = a^-$. Then $v_{k+l+1} = v_{k+l} + \delta a^- = v_k + (l+1)\delta a^-$ so (26) holds for $l \leq N(s_k, \tilde{a})$. When $l = N(s_k, \tilde{a})$, we have

$$v_{k+l} = v_k + N(s_k, \tilde{a})\delta a^- = v_k + \lfloor v_k/(\delta|a^-|) \rfloor \delta a^- \quad (27)$$

From (27) we then have

$$v_{k+l} \geq v_k + (v_k/\delta|a^-|)\delta a^- = 0. \quad (28)$$

Similarly, from (27) and recalling that $a^- < 0$ so $\lfloor v_k/(\delta|a^-|) \rfloor \delta a^- \leq (v_k/(\delta|a^-|) - 1)\delta a^-$,

$$v_{k+l} \leq v_k + (v_k/(\delta|a^-|) - 1)\delta a^- = -\delta a^-. \quad (29)$$

Then from (28), (29), and (22), we have $\tilde{u}_{dbl}(s_{k+l}) = -v_{k+l}/\delta$ so $v_{k+l+1} = v_{k+l} - \delta v_{k+l}/\delta = 0$ and it follows trivially by induction that $v_{k+l} = 0$ for all $l > N(s_k, \tilde{a})$.

We now show by induction that for nonnegative integers l with $l \leq N(s_k, \tilde{a})$,

$$p_{k+l} = p_k + \delta l v_k + \frac{l(l-1)}{2} \delta^2 a^-. \quad (30)$$

This holds trivially for $l = 0$. Suppose it holds for some l where $0 \leq l \leq N(s_k, \tilde{a}) - 1$. Then since $l(l-1)/2 + l = (l+1)l/2$,

$$\begin{aligned} p_{k+l+1} &= p_{k+l} + \delta v_{k+l} \\ &= p_k + \delta l v_k + \frac{l(l-1)}{2} \delta^2 a^- + \delta(v_k + \delta l a^-) \\ &= p_k + \delta(l+1)v_k + \frac{(l+1)l}{2} \delta^2 a^- \end{aligned}$$

Then (30) holds for $0 \leq l \leq N(s_k, \tilde{a})$. For $l = N(s_k, \tilde{a})$, note that $p_{k+l+1} = p_{k+l} + \delta v_{k+l} = p_{k+l} + \delta(v_k + \delta N(s_k, \tilde{a}) a^-) = \eta(s_k, \tilde{a})$. Since $v_{k+l+1} = 0$ for all $l > N(s_k, \tilde{a})$, $p_{k+l} = p_{k+N(s_k, \tilde{a})+1}$. Since $v_{k+l} \geq 0$ for all $l \geq 0$, p_{k+l} is a non-decreasing function so $p_{k+l} \leq \eta(s_k, N_k, \tilde{a})$ for all $l \geq 0$. Hence (a) and (b) hold.

We now show that η is continuous. Choose some positive integer M . It has already been shown in part (a) that if $M > v_k/\delta a^- + 1$ that $\eta(s_k, \tilde{a}) = p_{k+M}$. But the mapping $p_k \rightarrow p_{k+M}$ using the control law \tilde{u}_{dbl} in (22) is continuous because (22) and (21) are continuous. Then η is continuous on the set $\{s_k \in \mathbb{R}^{n_u} : v_k/\delta a^- + 1 < M\}$. Since M can be chosen to be arbitrarily large, η is continuous on \mathbb{R}^{n_s} .

We now prove that $\eta(s_k, \tilde{a}) = \eta(f(s_k, \tilde{u}_{dbl}(s_k, \tilde{a})), \tilde{a})$. Note again we are considering the case of $v_k \geq 0$ since the other case follows similarly. Denote $s_{k+1} \triangleq f(s_k, \tilde{u}_{dbl}(s_k, \tilde{a}))$.

Suppose $N(s_k, \tilde{a}) = 0$. Then $\eta(s_k) = p_k + \delta v_k$. Also, since $N(s_k, \tilde{a}) = 0$ we have $v_k < \delta|a^-|$, so given \tilde{u}_{dbl} in (22), $v_{k+1} = 0$. Then $N(s_{k+1}, \tilde{a}) = 0$ so $\eta(s_{k+1}) = p_k + \delta v_k$.

Suppose $N(s_k, \tilde{a}) \geq 1$. Then $N(s_{k+1}, \tilde{a}) = \lfloor (v_k + \delta a^-)/|\delta a^-| \rfloor = \lfloor (v_k + \delta a^-)/\delta a^- \rfloor = N(s_k, \tilde{a}) - 1$. Then

$$\begin{aligned} \eta(s_{k+1}, \tilde{a}) &= p_k + \delta v_k + \delta(N(s_k, \tilde{a}) - 1)(v_k + \delta a^-) \\ &\quad + \frac{(N(s_k, \tilde{a}) - 1)(N(s_k, \tilde{a}) - 2)}{2} \delta^2 a^- \\ &\quad + \delta(v_k + \delta a^- + \delta(N(s_k, \tilde{a}) - 1)a^-). \end{aligned}$$

Noting $(l-1)(l-2)/2 = l(l-1)/2 + 1 - l$, we have

$$\begin{aligned} \eta(s_{k+1}, \tilde{a}) &= p_k + \delta v_k + \delta N(s_k, \tilde{a})v_k + \delta^2 N(s_k, \tilde{a})a^- - \delta v_k - \delta^2 a^- \\ &+ \frac{N(s_k, \tilde{a})(N(s_k, \tilde{a}) - 1)}{2} \delta^2 a^- + \delta^2 a^- - N(s_k, \tilde{a})\delta^2 a^- \\ &+ \delta(v_k + \delta N(s_k, \tilde{a})a^-) + \delta^2 a^- - \delta^2 a^- \\ &= \eta(s_k, \tilde{a}). \end{aligned}$$

Finally, we show that as v_k increases, η increases. Consider $s_{a,k} = (p_{a,k}, v_{a,k})^T$ and $s_{b,k} = (p_{b,k}, v_{b,k})^T$ for $p_{a,k} = p_{b,k}$ and $v_{a,k} = v_{b,k} + \epsilon$ for some $\epsilon > 0$. From (26), $v_{a,k+l} \geq v_{v,k+l}$ for all integers $l \geq 0$. Then since $p_{a,k} = p_{b,k}$ and $v_{a,k+l} \geq v_{b,k+l}$ for all $l \geq 0$, $p_{a,k+l} \geq p_{b,k+l}$ for all $l \geq 0$. Then $\eta(s_{a,k}) \geq \eta(s_{b,k})$ follows from Lemma 5a. \square

By Lemma 5a, the output of η is where the position ends after using \tilde{u}_{dbl} for all time. Hence for $p_{min}, p_{max} \in \mathbb{R}$, let

$$h_{L,dbl}(s_k) = \min(p_k, \eta(s_k, \tilde{a})) - p_{min} \quad (31)$$

$$h_{H,dbl}(s_k) = p_{max} - \max(p_k, \eta(s_k, \tilde{a})) \quad (32)$$

Theorem 3. For the system (21), $h_{L,dbl}$ and $h_{H,dbl}$ defined in (31) and (32) are DT-ECBFs.

Proof. Choose s_k such that $h_{L,dbl}(s_k) \geq 0$. Denote s_{k+1} as the state after applying $\tilde{u}_{dbl}(s_k, \tilde{a})$ given dynamics (21).

If $v_k \geq 0$ then $p_{k+1} \geq p_k$. Further, by Lemma 5b, $p_k \leq \eta(s_k, \tilde{a})$. Given $a_k = \tilde{u}_{dbl}(s_k, \tilde{a})$, we have $v_{k+1} \geq 0$ so, again by Lemma 5b, $p_{k+1} \leq \eta(s_{k+1})$. Then $h_L(s_{k+1}) = p_{k+1} - p_{min} \geq p_k - p_{min} = h_L(s_k)$.

If $v_k < 0$ then similarly by Lemma 5b and given $\tilde{u}_{dbl}(s_k)$, $p_k \geq \eta(s_k, \tilde{a})$, $v_{k+1} \leq 0$, $p_{k+1} \geq \eta(s_{k+1}, \tilde{a})$. Then by Lemma 5c, $h_{L,dbl}(s_{k+1}) = \eta(s_{k+1}, \tilde{a}) - p_{min} = \eta(s_k, \tilde{a}) - p_{min} = h_{L,dbl}(s_k)$. The proof for (32) is similar. \square

Remark 2. From Lemma 5c, η is continuous. Hence $h_{L,dbl}$ and $h_{H,dbl}$ are continuous.

V. BARRIER FUNCTION FOR LANE MERGING AND ADAPTIVE CRUISE CONTROL

Consider a driving scenario where a vehicle is on a road with two lanes going in the same direction. Note [1] also analyzed this problem for lane keeping and adaptive cruise control. The approach here differs in that the barrier functions allow for changing lanes, account for multiple lead cars in multiple lanes, the dynamics are not linear in the control input, and the model is in discrete time. Deriving a barrier function in discrete time can be challenging because we cannot take derivatives with respect to time to find the minimum of a function. However, discrete time barrier functions do not need to be continuously differentiable so this provides some extra flexibility. In particular, in this section we use the fact that the maximum or minimum of barrier functions is a barrier function. See Corollary 1.

Consider a case where there are two lead vehicles as well as an autonomous vehicle with states $s_{j,k}$ for $j = 1, 2, 3$, respectively. Index $j = 3$ refers to the autonomous car while indexes $j = 1, 2$ refers to lead cars in lanes 1 and 2, respectively. The kinematic bicycle model vehicle with state

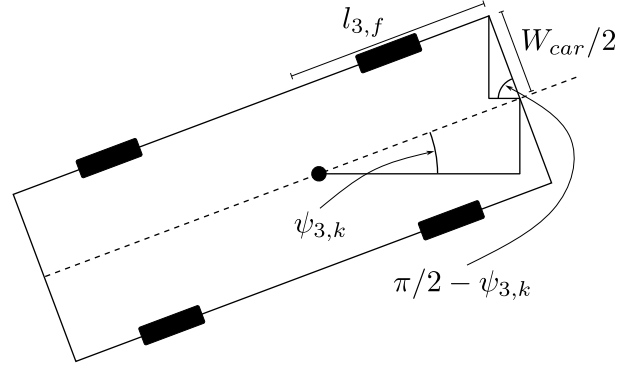


Fig. 3: Computing the lateral offset from the state so that the edge of the car does not exit a lane.

$s_{j,k} = (x_{j,k}, y_{j,k}, v_{j,k}, \psi_{j,k})^T$ is given by (see equation (2) of [35])

$$x_{j,k+1} = x_{j,k} + \delta v_{j,k} \cos(\psi_{j,k} + \beta(u_{2,j,k})) \quad (33a)$$

$$y_{j,k+1} = y_{j,k} + \delta v_{j,k} \sin(\psi_{j,k} + \beta(u_{2,j,k})) \quad (33b)$$

$$v_{j,k+1} = v_{j,k} + \delta u_{1,j,k} \quad (33c)$$

$$\psi_{j,k+1} = \psi_{j,k} + \delta \frac{v_{j,k}}{l_{j,r}} \sin(\beta(u_{2,j,k})) \quad (33d)$$

where $x_{j,k}$ ($y_{j,k}$) is the x (y)-position, $v_{j,k}$ is the speed, $\psi_{j,k}$ is the angle between the centerline of the road and the vehicle velocity, $\beta(u_{2,j,k}) = \tan^{-1}(\tan(u_{2,j,k})l_{j,r}/(l_{j,f} + l_{j,r}))$, $u_{1,j,k} \in [a_{min}, a_{max}]$ is the acceleration, $u_{2,j,k} \in [-u_{2,max}, u_{2,max}]$ is the front wheel steering angle, and $l_{j,f}$ ($l_{j,r}$) is the distance between the front (rear) axle and center of gravity. The state of the system is $s_j = ([s_{1,k}]^T, [s_{2,k}]^T, [s_{3,k}]^T)^T$.

For brevity let $b_{min} = \sin(\beta(-u_{2,max}))$ and $b_{max} = \sin(\beta(u_{2,max}))$. Then $\beta^{-1}(\sin^{-1}(\cdot))$ where $\beta^{-1}(\cdot) = \tan^{-1}(\tan(\cdot)(l_{j,f} + l_{j,r})/l_{j,r})$ is well defined for any value within $[b_{min}, b_{max}]$ given a small enough $u_{2,max}$. Let $\tilde{u}_{steer}(s_{3,k}) = 0$ for $v_{3,k} = 0$ and

$$\begin{aligned} \tilde{u}_{steer}(s_{3,k}) &= \\ &\beta^{-1}(\sin^{-1}(\min\{\max[-\psi_{3,k}l_{3,r}/(\delta v_{3,k}), b_{min}], b_{max}\})) \end{aligned} \quad (34)$$

otherwise. Let

$$\tilde{u}_3(s_{3,k}, \tilde{a}_3) = (\tilde{u}_{dbl}(s_{3,k}, \tilde{a}_3), \tilde{u}_{steer}(s_{3,k}))^T \quad (35)$$

for $\tilde{a}_3 = [a_3^-, a_3^+]^T$ for $a_3^- \in [u_{1,min}, 0)$, $a_3^+ \in (0, u_{1,max}]$ and for $\tilde{u}_{k,dbl}$ defined in (22).

Given the car position of $y_{3,k}$, the largest offset of the vehicle given a width W_{car} is given by (see Figure 3)

$$O(s_{3,k}) = l_{3,f} |\sin(\psi_{3,k})| + (W_{car}/2) |\cos(\psi_{3,k})|. \quad (36)$$

To stay in lane 1, the car must maintain $y_{3,k} \in [O(s_{3,k}), W_{lane} - O(s_{3,k})]$ where W_{lane} is the width of the lane. Similarly, to stay in lane 2, the car must maintain $y_{3,k} \in [W_{lane} + O(s_{3,k}), 2W_{lane} - O(s_{3,k})]$. Let

$$\begin{aligned} \rho_{L^1}(s_k) &= y_{3,k} - O(s_{3,k}) \\ \rho_{H^1}(s_k) &= W_{lane} - O(s_{3,k}) - y_{3,k} \\ \rho_{L^2}(s_k) &= y_{3,k} - O(s_{3,k}) - W_{lane} \\ \rho_{H^2}(s_k) &= 2W_{lane} - O(s_{3,k}) - y_{3,k}. \end{aligned}$$

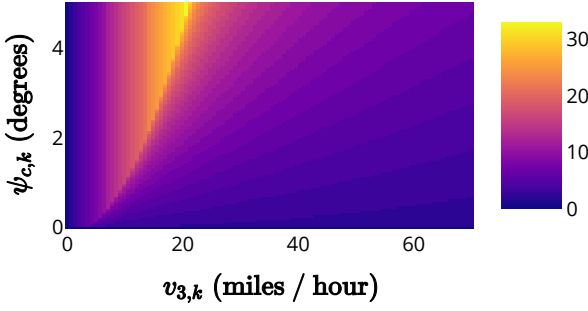


Fig. 4: The number of steps to evaluate a barrier function in (5) for keeping a safe distance from lane boundaries.

The subscript L^i (H^i) means the lower (higher) boundary for lane i for $i = 1, 2$. Construct $h_{L^1}, h_{H^1}, h_{L^2}$, and h_{H^2} via (5) using evasive maneuver $\zeta = \tilde{u}_3$ in (35) and safety functions $\rho_{L^1}, \rho_{H^1}, \rho_{L^2}$, and ρ_{H^2} , respectively. Then by Theorem 1 of [26], $h_{L^1}, h_{H^1}, h_{L^2}$, and h_{H^2} are barrier functions. While (5) requires an evaluation over an infinite horizon, given $\zeta = \tilde{u}_3$, $v_{3,k+l}$ will be zero within $N((y_{3,k}, v_{3,k})^T, \tilde{a}) + 1$ timesteps so (5) can be evaluated over $N((y_{3,k}, v_{3,k})^T, \tilde{a}) + 1$ timesteps. If $v_{3,k}$ is small, then $N((y_{3,k}, v_{3,k})^T, \tilde{a})$ will be small. If $v_{3,k}$ is large then $\psi_{3,k+l}$ will also be zero reasonably quickly (see (33d) and (34)). See Figure 4 for a computation of the number of timesteps required for a variety of settings of $v_{3,k}$ and $\psi_{3,k}$. The maximum number of steps is 33 over this range.

We now consider how to ensure that the car with state $s_{3,k}$ maintains a safe distance from the lead cars $s_{1,k}$ and $s_{2,k}$, the cars in lanes 1 and 2, respectively. The *lead car assumption* says that the lead cars stay in their lane, maintain a non-negative speed, car with index 1 and 2 are in lanes 1 and 2 respectively, and the lead cars do not turn.

Assumption 1. (Lead Car Assumption) For all integers k , $0 \leq y_{1,k} \pm W_{car} \leq W_{lane} \leq y_{2,k} \pm W_{car} \leq 2W_{lane}$, $\psi_{1,k} = \psi_{2,k} = 0$, and $v_{1,k} = v_{2,k} \geq 0$.

Under the lead car assumption, $u_{2,j,k} = 0$ so the dynamics of lead car $j = 1, 2$ is given by

$$\begin{aligned} x_{j,k+1} &= x_{j,k} + \delta v_{j,k} \\ v_{j,k+1} &= v_{j,k} + \delta u_{1,j,k}. \end{aligned}$$

Let $D_{lead} \geq 0$ be the minimum allowed intervehicle distance and τ_{head} the minimum allowed headway so that the distance from the lead and following car must satisfy $(x_{j,k} - x_{3,k} - D_{lead}) - v_{3,k}\tau_{head}$ for all k and $j = 1, 2$. The time headway distance is a common metric for safe distances in both barrier functions and MPC [1], [16]. For $j = 1, 2$ with $D_{lead} \geq 0$ and $\tau_{head} \geq 0$, let

$$\begin{aligned} \tilde{v}_{3,k} &= \max(0, v_{3,k}) \\ d_{j,lead}(s_k) &= \eta((x_{j,k}, \min(v_{j,k}, \tilde{v}_{3,k}))^T, (u_{1,min}, u_{1,max})) \\ &\quad - \eta((x_{3,k}, \tilde{v}_{3,k})^T, \tilde{a}_3) \\ h_{j,lead}(s_k) &= d_{j,lead}(s_k) - D_{lead} - \tilde{v}_{3,k}\tau_{head} \end{aligned} \quad (37)$$

Theorem 4. For a system with state $s_k = ([s_{1,k}]^T, [s_{2,k}]^T, [s_{3,k}]^T)^T$ where $s_{j,k}$ has dynamics in (33) for $j = 1, 2, 3$, suppose that the lead car assumption

holds. Then $h_{j,lead}$ defined in (37) for $j = 1, 2$ is a DT-ECBF.

Proof. For notational simplicity, we set $j = 1$ in this proof. The case of $j = 2$ follows similarly. Denote $\eta_{1,k}(v) \triangleq \eta((x_{1,k}, v)^T, (u_{1,min}, u_{1,max}))$ and $\eta_{3,k}(v) \triangleq \eta((x_{3,k}, v)^T, \tilde{a}_3)$. By the lead car assumption, $\psi_{1,k} = 0$ for all k . Vehicle 3 does not have control over the lead vehicles so we assume the worst case where $u_{1,j,k} = \tilde{u}_{dbl}(s_{1,k}, \tilde{a}_1)$ with $\tilde{a}_1 = (u_{1,min}, u_{1,max})^T$. Denote $v_{1,k+1} = v_{1,k} + \delta \tilde{u}_{dbl}((x_{1,k}, v_{1,k})^T, \tilde{a}_1)$ and $v_{3,k+1} = v_{3,k} + \delta \tilde{u}_{dbl}((x_{3,k}, v_{3,k})^T, \tilde{a}_3)$. We show that when vehicle 3 has control input given by (35), $h_{1,lead}$ satisfies (3).

Case 1: Suppose $v_{3,k} \leq 0$. Then with control input given by (35), $v_{3,k+1} \leq 0$ so $\tilde{v}_{3,k} = \tilde{v}_{3,k+1} = 0$. By the lead car assumption, $v_{1,k} \geq 0$ so $x_{1,k+1} \geq x_{1,k}$ so $\eta_{1,k+1}(0) = x_{1,k+1} \geq x_{1,k} = \eta_{1,k}(0)$. For similar reasons since $v_{3,k} \leq 0$, $\eta_{3,k+1}(0) \leq \eta_{3,k}(0)$. Then $h_{1,lead}(s_{k+1}) = \eta_{1,k+1}(0) - \eta_{3,k+1}(0) - D_{lead} \geq \eta_{1,k}(0) - \eta_{3,k}(0) - D_{lead} = h_{1,lead}(s_k)$.

Case 2: Suppose $v_{3,k} \geq 0$ so that given the control in (35), $v_{3,k} \geq v_{3,k+1} \geq 0$. From Lemma 5c, $\eta_{1,k+1}(v_{1,k+1}) = \eta_{1,k}(v_{1,k})$ and $\eta_{3,k+1}(v_{3,k+1}) = \eta_{3,k}(v_{3,k})$.

Case 2a: Suppose $v_{1,k} \leq v_{3,k}$. Then $v_{1,k+1} \leq v_{3,k+1}$ because $\tilde{u}_{dbl}((x_{3,k}, v_{3,k})^T, \tilde{a}_3) \geq \tilde{u}_{dbl}((x_{1,k}, v_{1,k})^T, \tilde{a}_1)$. Then

$$\begin{aligned} h_{1,lead}(s_{k+1}) &= \eta_{1,k+1}(v_{1,k+1}) - \eta_{3,k+1}(v_{3,k+1}) - D_{lead} - \tau_{head}v_{3,k+1} \\ &\geq \eta_{1,k}(v_{1,k}) - \eta_{3,k}(v_{3,k}) - D_{lead} - \tau_{head}v_{3,k} \\ &= h_{1,lead}(s_k). \end{aligned}$$

Case 2b: If $v_{1,k} \geq v_{3,k} \geq 0$ then $\eta_{1,k}(v_{1,k}) \geq \eta_{1,k}(v_{3,k})$ by Lemma 5d. If $v_{1,k+1} < v_{3,k+1}$, then using Lemma 5c,

$$\begin{aligned} h_{1,lead}(s_{k+1}) &= \eta_{1,k+1}(v_{1,k+1}) - \eta_{3,k+1}(v_{3,k+1}) - D_{lead} - v_{3,k+1}\tau_{head} \\ &\geq \eta_{1,k}(v_{1,k}) - \eta_{3,k}(v_{3,k}) - D_{lead} - v_{3,k}\tau_{head} \\ &\geq \eta_{1,k}(v_{3,k}) - \eta_{3,k}(v_{3,k}) - D_{lead} - v_{3,k}\tau_{head} \\ &= h_{1,lead}(s_k). \end{aligned}$$

Consider now when $v_{1,k+1} \geq v_{3,k+1}$. For notational simplicity, denote $\tilde{u}_{dbl,1,k}(v) \triangleq \tilde{u}_{dbl}((x_{1,k}, v)^T, \tilde{a}_1)$. Then since $v_{1,k} > v_{3,k} \geq 0$,

$$\tilde{u}_{dbl,1,k}(v_{1,k}) \leq \tilde{u}_{dbl,1,k}(v_{3,k}). \quad (38)$$

Then using (38) and that $\tilde{u}_{dbl,1,k}(v_{3,k}) \leq \tilde{u}_{dbl}((x_{3,k}, v_{3,k})^T, \tilde{a}_3)$,

$$v_{3,k} + \delta \tilde{u}_{dbl,1,k}(v_{1,k}) \leq v_{3,k} + \delta \tilde{u}_{dbl,1,k}(v_{3,k}) \leq v_{3,k+1}. \quad (39)$$

From Lemma 5c, $\eta_{1,k}(v_{3,k}) = \eta_{1,k+1}(v_{3,k} + \delta \tilde{u}_{dbl,1,k}(v_{1,k}))$. From this, (39), and Lemma 5d we have

$$\eta_{1,k}(v_{3,k}) = \eta_{1,k+1}(v_{3,k} + \delta \tilde{u}_{dbl,1,k}(v_{1,k})) \leq \eta_{1,k+1}(v_{3,k+1}). \quad (40)$$

Then using (40), noting that $v_{3,k+1} \leq v_{3,k}$, and that Lemma 5c implies $\eta_{3,k}(v_{3,k}) = \eta_{3,k+1}(v_{3,k+1})$, we have

$$\begin{aligned} h_{1,lead}(s_k) &= \eta_{1,k}(v_{3,k}) - \eta_{3,k}(v_{3,k}) - D_{lead} - \tau_{head}v_{3,k} \\ &\leq \eta_{1,k+1}(v_{3,k+1}) - \eta_{3,k+1}(v_{3,k+1}) - D_{lead} - \tau_{head}v_{3,k+1} \\ &= h_{1,lead}(s_{k+1}). \end{aligned}$$

□

The vehicle must also obey speed limits so let $v_{lim} \geq 0$ and

$$h_{spd}(s_k) = v_{lim} - \max(0, v_{3,k}), \quad (41)$$

which is a barrier function by a straightforward calculation using the control input (35).

Given Corollary 1 and Theorem 3 of [26], we now use barrier function composition to simultaneously satisfy the safety constraints. For brevity, denote $\max(\cdot, \cdot)$ by $\cdot \wedge \cdot$ and $\min(\cdot, \cdot)$ as $\cdot \vee \cdot$. Additionally, we drop the function argument so $h = h_{spd} \wedge h_{turn}$ means that given $s_k \in \mathbb{R}^{n_s}$, $h(s_k) = h_{spd}(s_k) \wedge h_{turn}(s_k)$. Let

$$h_{car} = \left[h_{spd} \wedge h_{L^1} \wedge h_{H^2} \right] \wedge \left[(h_{H^1} \wedge h_{1,lead}) \vee (h_{L^2} \wedge h_{2,lead}) \vee (h_{1,lead} \wedge h_{2,lead}) \right].$$

The first bracketed $[\cdot]$ term ensures the car satisfies speed limits and stays within the road limits. The second bracketed term ensures one of the following holds: (1) the car stays in the first lane and a safe distance from the lead car in the first lane, (2) the car stays in the second lane and a safe distance from the lead car in the second lane, or (3) the car stays a safe distance from both lead cars but can change lanes.

VI. EXPERIMENTS

A. Environments and Algorithms

In Sections III and V, we derived barrier functions for fixed wing aircraft and self driving cars. Although the direct computation of (4) is infeasible for non-convex systems, we consider three efficient alternatives. First, we use a Lagrangian computation, called BF LAG, which has been employed previously in constrained deep learning problems (e.g. [13], [19]). In this approach, let $u_\phi : \mathbb{R}^{n_s} \times \mathbb{R}^{n_u} \rightarrow U$ be a neural network parameterized by ϕ . Given a state and nominal control input pair, the Lagrangian is

$$\mathcal{L}(s_k, \hat{u}_k) = \frac{1}{2} \|\hat{u}_k - u_\phi(s_k, \hat{u}_k)\|^2 - \kappa c_h(s_k, u_\phi(s_k, \hat{u}_k)) \quad (42)$$

where $\kappa \geq 0$ is a Lagrange multiplier. We update ϕ by minimizing (42) via gradient descent. Similarly, given a cost, we update κ via $\kappa = \max(0, \kappa - r c_h(s_k, u_\phi(s_k)))$ where $r > 0$ is a learning rate (we set $r = 1000$ in our experiments). We additionally take the minimum of c_h and 0.0001 in (42) so that when minimizing the expectation of the Lagrangian in (42), the average constraint is less likely to be positive when u_ϕ has some constraint violations in the dataset. Because there is no guarantee that u_ϕ outputs a safe action, we also include a line search for the lowest cost, safe action u_l between \hat{u}_k and \tilde{u}_k , the known safe action. See (14) and (35) for \tilde{u}_k given fixed-wing and car systems, respectively. Further, even if u_ϕ outputs a safe action, there is no guarantee that the action is optimal with respect to (4), so we include a line search between \hat{u}_k and $u_\phi(s_k, \hat{u}_k)$ to find the lowest cost but safe action $u_{\phi,l}$ along the line between \hat{u}_k and $u_\phi(s_k, \hat{u}_k)$. If both \hat{u}_k and $u_\phi(s_k, \hat{u}_k)$ are unsafe, $u_{\phi,l}$ can be unsafe, so in this case we apply u_l .

Otherwise we apply $u_{\phi,l}$ or u_l , whichever has the lowest cost for (4). The two other alternative overrides we evaluate are u_l (called BF Line) and \tilde{u}_k (called BF SINGLE).

For RL baselines, we compare a barrier override to algorithms discussed for the GUARD Safe RL benchmark [36]. In particular, the baselines consist of Trust Region Policy Optimization (TRPO) [37], Unrolling Safety Layer (USL) [24], Constrained Policy Optimization (CPO) [18], Feasible Actor Critic (FAC) [19], and LAG (TRPO with a Langrian cost term). TRPO is the unconstrained baseline to measure the peak performance that can be achieved without considering safety. USL does an online action correction by passing the action through a cost network and applying back propagation to update the action until the cost is below a threshold. CPO approximates a trust region constrained optimization of surrogate functions with guaranteed improvement bounds. LAG applies a policy loss that includes a cost correction with a coefficient that increases when the cost exceeds a threshold. Finally, FAC extends the Lagrangian approach by making the cost correction coefficient dependent on the state.

We evaluate the barrier function overrides against these baselines in two environments for which we have derived barrier functions. For every state that violates the safety condition, the agent gets a cost of 1. Similarly, an episode is considered unsafe if any state during the episode is unsafe. To account for floating point error, we only count a state as violating a constraint if it is more than 10^{-6} beyond a given safety limit. We include the number of unsafe episodes experienced during training as it provides an interpretable cost budget over the course of training, similar e.g. [21].

In our first environment, we evaluate whether the barrier function in (17) can allow fixed wing aircraft to stay within a safe flight envelope while using RL to learn to do waypoint following (see Fig. 1). We use aircraft parameters from [29], [38] and choose reasonable values for μ_{max} , v_{min} , v_{max} , and z_{min} (see Table I). For the waypoint objective, we start the aircraft at $x_0 = (17.5, 0, 0, 0, 0, 500)^T$ (velocity is meters per second, angles are in radians, and positions are in meters) and have 5 waypoints $w_i \in \mathbb{R}^3$ located at $w_{i+1} = w_i + (100, U_{i,y}, U_{i,z})^T$ where $w_0 = x_0$ and $U_{i,y}, U_{i,z}$ are samples from a uniformly distributed random variable over the range of $[-25, 25]$ meters for $i = 1, \dots, 5$. The observation consists of scaled velocity (i.e. $(v_k - v_{min})/(v_{min} - v_{max})$), scaled γ_k (i.e. γ_k/γ_{max}), $\sin \psi_k$, $\cos \psi_k$, the vector to the next waypoint relative to the current position (i.e. $(w_j - (x_k, y_k, z_k)^T)/O$ where j is the index of the next waypoint and $O = 50$ is a scaling factor), and the scaled change to each subsequent waypoint (i.e. $(w_{l+1} - w_l)/O$ for $l = j + 1, \dots, 6$). Because the observation is a fixed size, we also append a valid flag and fill the waypoint vectors with zeros when $l + 1 > 5$. At every timestep, the agent receives a reward of 0.01 times the change in distance to the next waypoint. A waypoint w_i is reached when x_k is greater than the x -component of w_i . At this point $e^{-d_{i,k}/25}$ is added to the reward where $d_{i,k}$ is the distance of the vehicle to w_i . We set $\delta = 0.1$ and end an episode after 1000 timesteps, the last waypoint is reached, it has taken more than 10 seconds to reach the next waypoint, or the vehicle hits the ground.

Our second environment focuses on lane merging with adaptive cruise control for self-driving cars. In this scenario, the car under control is in a two lane road with lead cars in both of the lanes. The lead car initial offset is chosen from a uniform distribution between 100 and 500 meters with initial speed between 0 and 70 miles per hour. If an initial lead car state results in a system state s_0 where in $h_{car}(s_0) < 0$ then we sample again until a safe initial condition is found. The lead car behavior continues at this speed for a uniformly sampled time varying between 0 and 5 seconds at which point it selects a new target speed between 0 and 70 miles per hour, applying maximum acceleration or deceleration to achieve this speed. The autonomous vehicle must learn to keep a safe distance behind the lead car so that even in the rare case that the lead car decelerates maximally to a stop, the autonomous vehicle can still avoid a collision by similarly braking or by changing lanes, provided the vehicle in the other lane is far enough ahead to allow this to be done safely. When the autonomous vehicle passes a lead vehicle, we spawn a new lead vehicle in the same lane using the same logic as the beginning of the episode. The autonomous vehicle has a speed goal of $v_{tgt} = 70$ miles per hour which is the same as the speed limit. It starts with an initial speed of 95% of the speed target. The observation consists of the vector

$$obs(s_k) = \begin{bmatrix} (d_{1,k} - 500)/500 \\ (d_{2,k} - 500)/500 \\ (y_{3,k} - W_{lane})/W_{lane} \\ (v_{1,k} - v_{tgt})/v_{tgt} \\ (v_{2,k} - v_{tgt})/v_{tgt} \\ (v_{3,k} - v_{tgt})/v_{tgt} \\ \sin \psi_{3,k} \\ \cos \psi_{3,k} \end{bmatrix}.$$

where $d_{j,k} = x_{j,k} - x_{3,k}$ for $j = 1, 2$. The reward is $r_k = 1 - |v_{3,k} - v_{tgt}|/v_{tgt}$ and the episode ends when the distance to the lead vehicle is less than D_{lead} , the vehicle has exited the road, or 1000 timesteps have elapsed. We use car parameters from [1], [35] and choose reasonable values for D_{lead} , v_{lim} , W_{lane} , and W_{car} (see Table II).

B. Results Relative to Safe RL Baselines

Results for the UAV environment are shown in Figure 5 which plots performance of the barrier function override using u_ϕ (called BF Lag) compared to the RL baselines. As expected, TRPO has the highest performance but as discussed in the next paragraph, also has the highest cost. USL has similar initial performance to TRPO because it has a burn-in period for the first two million steps where the safety override is inactive. However, once the safety override activates, performance deteriorates without improving safety. In two of the cases (LAG, CPO), the baseline cannot solve the task while the final baseline, FAC, learns to reduce unsafe behavior while producing significantly lower reward than TRPO.

Similarly, for cost, TRPO maintains a high cost throughout training. This is partly because the waypoints can be placed outside of what is feasible for the flight envelope but also that exceeding the speed limit increases the maximum discounted reward. Comparing reward and cost, there is a clear tradeoff

TABLE I: Fixed Wing UAV parameters

Parameter	Value	Units	Description
ρ	1.2251	kg/m^3	air density
W	68.68	N	weight
S	1.058	m^2	wing surface area
T_{max}	20.60	N	maximum thrust
$[n_{min}, n_{max}]$	$[-1.0, 2.5]$	unitless	min/max lift factor
C_{d0}	0.02544	unitless	parasitic drag coefficient
k	0.059	unitless	induced drag coefficient
μ_{max}	30	deg	max bank angle
$[v_{min}, v_{max}]$	$[15, 20]$	m/s	min/max speed
z_{min}	400	m	altitude floor
λ	0.5	unitless	see (3)

amongst the baselines as algorithms that achieve lower cost also achieve less reward. The only baselines to approximate zero cost (LAG and CPO) do so only near the end of training and do not solve the task. An interesting comparison is cost to the number of unsafe episodes. Notably, all baselines encounter many unsafe episodes, meaning that there is at least one state that is unsafe. This occurs because although the safety aware baselines make an attempt to have lower cost, they still have safety violations so their employment for safety critical applications is limited.

On the other hand, BF LAG achieves both high reward and zero cost during training where the reward is comparable to the unconstrained baseline and the cost is significantly improved over any of the baselines. In particular, BF LAG allows the RL system to achieve a higher reward than any of the constrained baselines while having a comparable reward to the unconstrained baseline TRPO. Notably, every baseline has at least 10,000 unsafe episodes whereas BF LAG has zero. It is likely that BF LAG achieves less reward per episode than the unconstrained baseline because we purposefully place waypoints outside of what is achievable within the safe flight envelope. For instance, given a max pitch of 10 degrees and 100 meters between waypoints, the maximum altitude change is given by $100 \sin(\psi_{max}) \approx 17$ meters, which is less than the limits of how much altitude difference there can be between waypoints of 25 meters.

In the car environment, an episode can be quickly ended by running off the road. This leads to non-intuitive results as the unconstrained baseline has high cost but also the least number of unsafe episodes of all the baselines. Because unsafe behavior means that the episode ends and the future rewards goes to zero, the unconstrained baseline learns relatively safe behavior in terms of catastrophic outputs (e.g. the lead car distance is less than D_{lead} or running off the road). At the same time, it ignores unsafe behavior that does not end the episode (going faster than the speed limit, getting closer than the time to collision limit). In other words, it learns to avoid behaviors that lead to catastrophic outcomes while allowing ones that have no effect on the reward. Other safe baselines appear to have the opposite approach. Because they are trained to avoid high cost, they learn to create catastrophic outcomes because those scenarios lead to a cost of 1 rather than keeping the episode going and inducing high costs from keeping the episode going. Results are in Figure 6. On the other hand, BF LAG does not suffer from this tuning challenge as it achieves

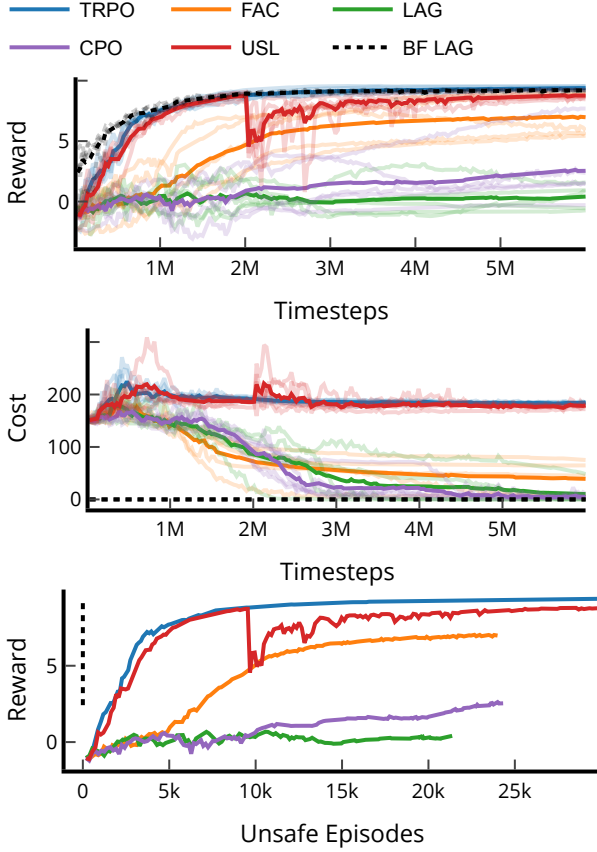


Fig. 5: Results in the waypoint following environment for a fixed wing UAV. (top) Reward as a function of episode sample, (middle) Cost as a function of episode sample, (bottom) Reward vs cumulative number of unsafe episodes. In the top and middle plots, faded lines show the outcomes of the five repeated experiments for a given algorithm while non-faded lines represent the mean of these experiments.

TABLE II: Car parameters

Parameter	Value	Units	Description
l_f	1.17	m	front distance
l_r	1.77	m	rear distance
$[u_{1,min}, u_{1,max}]$	$[-2.87, 2.87]$	m	min/max lead acceleration
\tilde{a}_3	$[2.86, 2.86]$	m	min/max acceleration
$[u_{2,min}, u_{2,max}]$	$[-1, 1]$	deg	min/max steering angle
τ	1.8	sec	time to collision
W_{car}	1.83	m	car width
W_{lane}	3.6	m	lane width
λ	0.5	unitless	see (3)

high reward and zero cost. Its initial high performance is due to it being able to keep episodes going the full 1000 timesteps. After this it learns to effectively pass cars to achieve speeds close to the target speed without having a collision.

C. Results of Barrier Override Alternatives

While BF LAG (the controller u_ϕ described in Section VI-A) is theoretically motivated by the Karush-Kuhn-Tucker

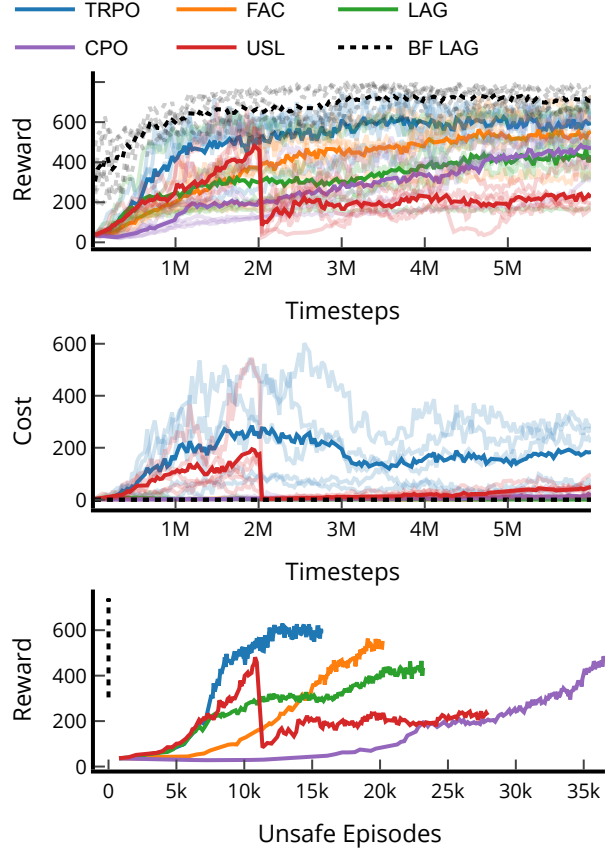


Fig. 6: Results in car environment. (top) Reward as a function of episode sample, (middle) Cost as a function of episode sample, (bottom) Reward vs cumulative number of unsafe episodes. In the top and middle plots, faded lines show the outcomes of the five repeated experiments for a given algorithm while non-faded lines represent the mean of these experiments.

conditions [39], it nevertheless has some disadvantages. First, choosing the initial value for the Lagrange multiplier κ and the associated learning rate can be difficult as it is affected by differences in scaling for the objective and constraint. This can be solved by hyperparameter tuning but this is unlikely to generalize across environments or even while training in a single environment [40]. For instance, in [36], the initial value and learning rate for the Lagrange multiplier is 0 and 0.005, respectively, for FAC whereas we find an initial value and learning rate of 10 and 1000 work better for u_ϕ . If the multiplier is too small, then u_ϕ may train too slowly to learn safe actions. On the other hand, if it is too large, u_ϕ may be conservative and not approximate \hat{u}_k particularly well. A second challenge of the Lagrange approach is that it violates the Markov assumption when training the RL policy which is a theoretical challenge for RL (discussed e.g. in [41]). To see how the Markov assumption is violated, note that when there is an override, the system has dynamics $f(s_k, u_\phi(s_k))$ and since $u_\phi(s_k)$ is changing due to updates from minimizing (42), the dynamics are changing as well. Third, training u_ϕ will slow down learning as the additional backpropagation adds

computational overhead. Fourth, there is no guarantee that u_ϕ will output a safe action even if s_k is such that $h(s_k) \geq 0$ (see Figure 9). Similarly, if u_ϕ outputs a safe action, there is no guarantee that the output is the closest possible $u_k \in U$ to \hat{u}_k such that $c_h(s_k, u_\phi(s_k, \hat{u}_k)) \geq 0$. This necessitates the line search discussed above for BF LAG. Similar to the third issue, the line search implies a higher computational overhead as it involves additional constraint computations which can be computationally intensive when either the dynamics in (1) or the barrier function have a significant computational burden. Finally, since u_ϕ is a neural network, interpreting its output is difficult. For a safety critical application, particularly where humans are involved, having a predictable override can increase interpretability and explainability as these factors are critical for trust [42]. Consider for instance a self-driving car example. A known override that the car will decelerate at a known rate and steer so that the car is parallel to the road is more interpretable than an override that is a neural network.

Figures 5 and 6 indicate that barrier functions can enable safe control overrides even when time is discrete or the dynamics are non-convex in the control input. We now compare the theoretically motivated override u_ϕ with more computationally efficient and more easily tuned overrides u_l (BF Line) and \tilde{u} (BF Single) in Figure 7. Surprisingly, the performance of BF LAG is nearly the same as BF Line and BF Single for the fixed wing environment (top plot of Figure 7) and in either environment, BF Single has similar performance to the top performing baselines. This is the case even though the distance between the override and the nominal control value is significantly smaller for BF Lag than BF Single (top middle plot of Figure 7). Given the relatively large distance of the override to the nominal, one would expect that, for all else equal, the deployed action would have a high standard deviation, since it may be switching between the nominal and conservative override of \tilde{u}_k . From the bottom middle plot of Figure 7 though, this is not the case, as BF Single actually has the lowest action standard deviation. Further, in the bottom plot of Figure 7, BF Single also has the least percentage of overrides of the alternatives. We posit from this that what is actually happening is that the RL system has learned that the BF Single override is significant and adapts the policy so that it avoids having an override take place. In other words, for the fixed wing environment, having an override that better approximates (4) does not yield much benefit because the RL system compensates for suboptimal solutions to (4).

On the other hand, Figure 8 shows that BF Lag does have benefits over BF Single in the car environment. However, even in this case, BF Single still matches the performance of the highest performing baseline (TRPO). Noting the significant number of violations for any of the RL baselines, it appears that being able to specify a barrier function for a system is sufficient for high performance safety assurance for both the fixed wing and car environments. An optimal computation of (4) is not necessary to beat cost aware RL even for discrete time, non-convex systems for the evaluated environments.

This observation has implications for RL deployment as there are significant downsides to employing BF Lag discussed above. Here we focus on the computational burden that BF Lag

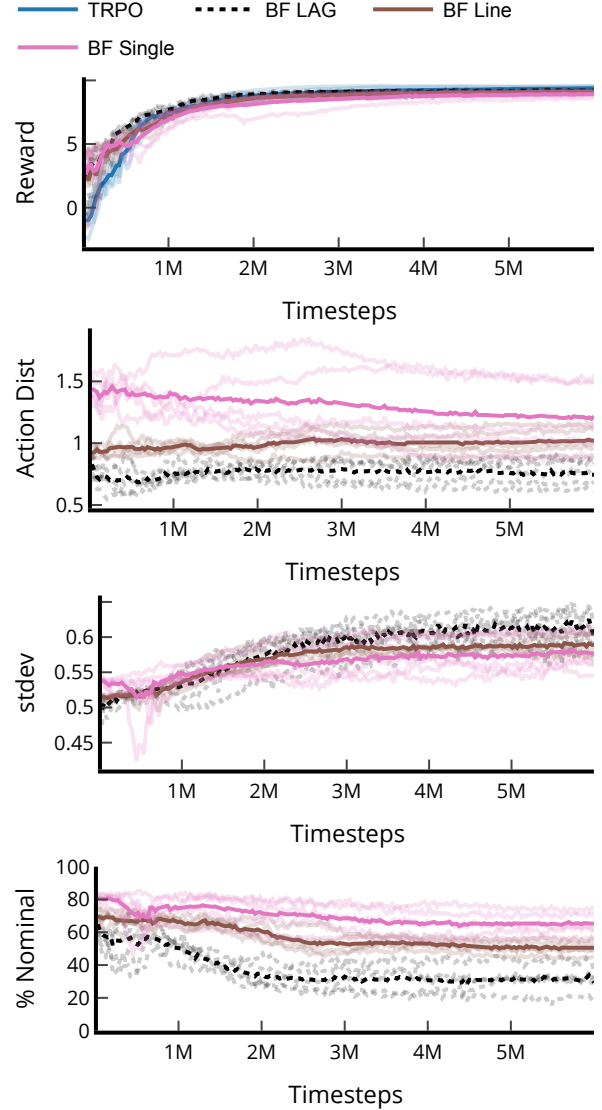


Fig. 7: A comparison of approximate barrier function overrides in the fixed wing UAV environment. (top) Reward as a function of episode sample, (top middle) Average distance of the override to the nominal control value, (bottom middle) Standard deviation of the control value. (bottom) Percentage of actions where the nominal override is used rather than an override. Faded lines show the outcomes of the five repeated experiments for a given algorithm while non-faded lines represent the mean of these experiments.

induces. RL often has a set of hyperparameters that must be tuned so avoiding also tuning the Lagrangian initial value and learning rate is a significant benefit of BF Single even if it results in somewhat less performance in the car environment. In addition, there is a significant computational overhead of BF Lag, primarily due to additional computations of the constraint (see Figure 4). In Table III we compare the computation times of BF Single and BF Lag, finding that BF Single training times are 1.7 and 3.0 times faster than BF Lag for the fixed-wing and car environments, respectively. In both environments, the key difference is that BF Single does less constraint calculations

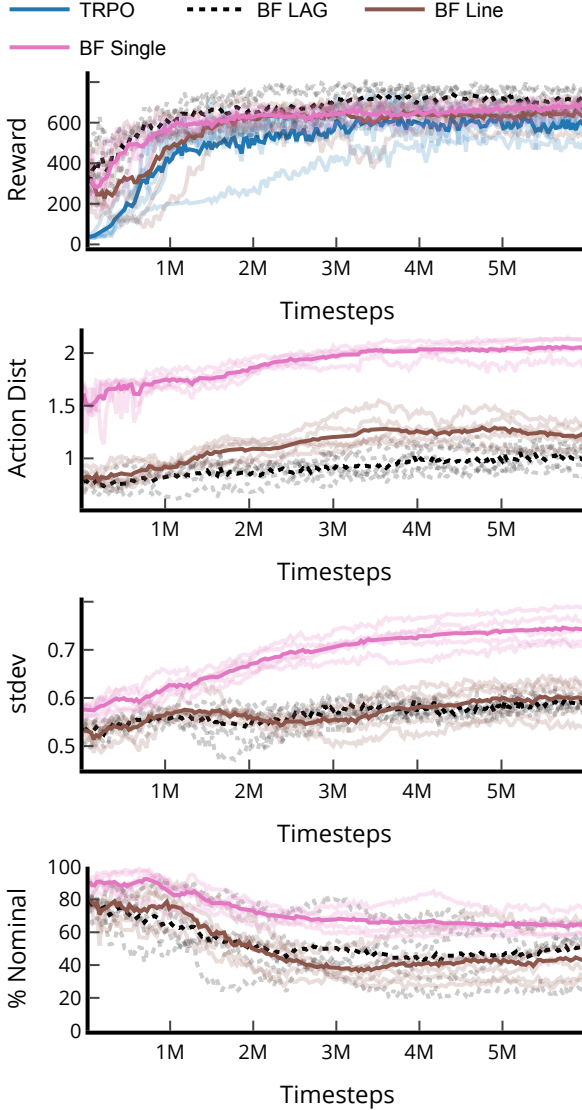


Fig. 8: A comparison of approximate barrier function overrides in the car environment. (top) Reward as a function of episode sample, (top middle) Average distance of the override to the nominal control value, (bottom middle) Standard deviation of the control value. (bottom) Percentage of actions where the nominal override is used rather than an override. Faded lines show the outcomes of the five repeated experiments for a given algorithm while non-faded lines represent the mean of these experiments.

and this is magnified in the car environment because the barrier function is more computationally intensive. The reason for this is the multi-step horizon in computing h_{L^1} , h_{L^2} , h_{H^1} , and h_{H^2} which causes c_h to become a bottleneck both in the forward pass as well as the backward pass of \mathcal{L} . In particular, because u_ϕ has no assurance that it will output a safe action (see Figure 9), we must include a line search to ensure that a safe override always occurs. Whether BF Lag has any beneficial effect on performance appears to be environment specific. However, given the downsides of BF Lag and the strong performance of BF Single relative to RL baselines, this makes BF Single a

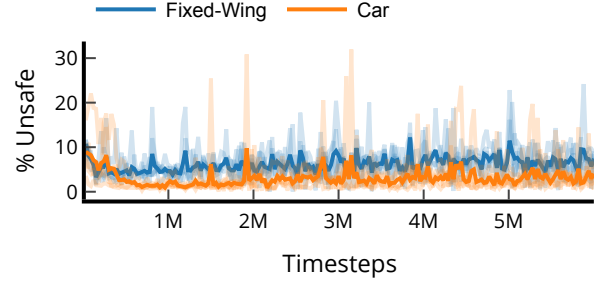


Fig. 9: The percentage of cases where u_ϕ (BF Lag) outputs an unsafe action.

TABLE III: Cumulative computation times in seconds per training epoch broken into data generation and training phases. Training is done on a Intel(R) Core(TM) i7-8700 CPU (3.20GHz) cpu. Gpu acceleration did not speed up training because the neural networks are relatively small.

		FW		Car	
		BF Lag	BF Single	BF Lag	BF Single
Gen Data	\hat{u}_k	9.3	9.1	9.3	9.1
	c_h	10.2	1.1	33.3	4.4
	Env Step	4.6	4.5	3.9	3.9
	h	0.5	0.5	3.4	3.3
	u_ϕ	3.2		2.3	
	\tilde{u}_k	0.5	0.1	0.7	0.3
Train	\mathcal{L} back	0.9		11.9	
	c_h fwd	0.2		7.1	
	Nominal	4.7	4.6	4.6	4.5
	u_ϕ fwd	0.4		0.4	
	h fwd	0.0		0.1	
		\mathcal{L} fwd	0.0	0.1	
Gen Data Total		28.2	15.3	52.9	21.1
Train Total		6.3	4.6	24.2	4.5
Total		34.5	19.9	77.1	25.5

reasonable approach for computing an override for non-convex problems when an override is included in RL training so that the RL system can incorporate the effect of the override in developing a policy.

VII. CONCLUSION

In this paper we have discussed issues with applying barrier functions to RL. In particular, although RL can be applied to dynamics that are non-convex in the control input, this can make computing an override with a barrier function computationally intractable. After deriving barrier functions for two systems that are non-convex in the control input, namely fixed wing aircraft and self-driving cars, we demonstrated that approximations of an optimal override are a computationally efficient way to ensure safety while preserving the performance capabilities of an RL system. In our comparison to safe RL baselines for fixed wing aircraft and self-driving cars, a barrier function with an approximate safe override has zero safety violations while having comparable or better performance relative to model free RL approaches. This suggests that barrier functions can be applied to non-convex systems while retaining the performance benefits of an RL system.

ACKNOWLEDGEMENTS

The authors would like to thank the Georgia Tech Research Institute for funding this research out of Independent Research and Development (IRAD) funds. Additionally, the authors would like to thank Dr. Klimka Kasraie for her valuable feedback on this paper.

REFERENCES

- [1] A. D. Ames, X. Xu, J. W. Grizzle, and P. Tabuada, "Control barrier function based quadratic programs for safety critical systems," *IEEE Transactions on Automatic Control*, vol. 62, no. 8, pp. 3861–3876, 2016.
- [2] A. D. Ames, S. Coogan, M. Egerstedt, G. Notomista, K. Sreenath, and P. Tabuada, "Control barrier functions: Theory and applications," in *2019 18th European control conference (ECC)*. IEEE, 2019, pp. 3420–3431.
- [3] K. DeMarco, E. Squires, M. Day, and C. Pippin, "Simulating collaborative robots in a massive multi-agent game environment (SCRIMMAGE)," in *Int. Symp. on Distributed Autonomous Robotic Systems*, 2018.
- [4] T. Binazadeh and M. A. Rahgoshay, "Robust output tracking of a class of non-affine systems," *Systems Science & Control Engineering*, vol. 5, no. 1, pp. 426–433, 2017.
- [5] A. Narang, "Analysis and control of non-affine, non-standard, singularly perturbed systems," Ph.D. dissertation, Texas A&M University, 2012.
- [6] A. Agrawal and K. Sreenath, "Discrete control barrier functions for safety-critical control of discrete systems with application to bipedal robot navigation," in *Robotics: Science and Systems*, vol. 13. Cambridge, MA, USA, 2017.
- [7] P. Rabiee and A. Safari, "Safe exploration in reinforcement learning: training backup control barrier functions with zero training time safety violations," *arXiv preprint arXiv:2312.07828*, 2023.
- [8] R. Cheng, G. Orosz, R. M. Murray, and J. W. Burdick, "End-to-end safe reinforcement learning through barrier functions for safety-critical continuous control tasks," in *Proceedings of the AAAI conference on artificial intelligence*, vol. 33, no. 01, 2019, pp. 3387–3395.
- [9] E. Squires, R. Konda, P. Pierpaoli, S. Coogan, and M. Egerstedt, "Safety with limited range sensing constraints for fixed wing aircraft," in *2021 IEEE International Conference on Robotics and Automation (ICRA)*. IEEE, 2021, pp. 9065–9071.
- [10] S. Pateria, B. Subagdja, A.-h. Tan, and C. Quek, "Hierarchical reinforcement learning: A comprehensive survey," *ACM Computing Surveys (CSUR)*, vol. 54, no. 5, pp. 1–35, 2021.
- [11] Y. Zhang, S. Walters, and X. Xu, "Control barrier function meets interval analysis: Safety-critical control with measurement and actuation uncertainties," in *2022 American Control Conference (ACC)*. IEEE, 2022, pp. 3814–3819.
- [12] J. Zeng, B. Zhang, and K. Sreenath, "Safety-critical model predictive control with discrete-time control barrier function," in *2021 American Control Conference (ACC)*. IEEE, 2021, pp. 3882–3889.
- [13] Y. Yang, Y. Jiang, Y. Liu, J. Chen, and S. E. Li, "Model-free safe reinforcement learning through neural barrier certificate," *IEEE Robotics and Automation Letters*, vol. 8, no. 3, pp. 1295–1302, 2023.
- [14] T. Gurriet, M. Mote, A. D. Ames, and E. Feron, "An online approach to active set invariance," in *2018 IEEE Conference on Decision and Control (CDC)*. IEEE, 2018, pp. 3592–3599.
- [15] E. Squires, P. Pierpaoli, R. Konda, S. Coogan, and M. Egerstedt, "Composition of safety constraints for fixed-wing collision avoidance amidst limited communications," *Journal of Guidance, Control, and Dynamics*, vol. 45, no. 4, pp. 714–725, 2022.
- [16] A. Katriniok, E. Shakheshi, and W. Heemels, "Discrete-time control barrier functions for guaranteed recursive feasibility in nonlinear mpc: An application to lane merging," in *2023 62nd IEEE Conference on Decision and Control (CDC)*. IEEE, 2023, pp. 3776–3783.
- [17] R. Cheng, M. J. Khojasteh, A. D. Ames, and J. W. Burdick, "Safe multi-agent interaction through robust control barrier functions with learned uncertainties," in *2020 59th IEEE Conference on Decision and Control (CDC)*. IEEE, 2020, pp. 777–783.
- [18] J. Achiam, D. Held, A. Tamar, and P. Abbeel, "Constrained policy optimization," in *International conference on machine learning*. PMLR, 2017, pp. 22–31.
- [19] H. Ma, Y. Guan, S. E. Li, X. Zhang, S. Zheng, and J. Chen, "Feasible actor-critic: Constrained reinforcement learning for ensuring statewise safety," *arXiv preprint arXiv:2105.10682*, 2021.
- [20] Y. Luo and T. Ma, "Learning barrier certificates: Towards safe reinforcement learning with zero training-time violations," *Advances in Neural Information Processing Systems*, vol. 34, pp. 25 621–25 632, 2021.
- [21] B. Thananjeyan, A. Balakrishna, S. Nair, M. Luo, K. Srinivasan, M. Hwang, J. E. Gonzalez, J. Ibarz, C. Finn, and K. Goldberg, "Recovery rl: Safe reinforcement learning with learned recovery zones," *IEEE Robotics and Automation Letters*, vol. 6, no. 3, pp. 4915–4922, 2021.
- [22] K. Srinivasan, B. Eysenbach, S. Ha, J. Tan, and C. Finn, "Learning to be safe: Deep rl with a safety critic," *arXiv preprint arXiv:2010.14603*, 2020.
- [23] N. C. Wagener, B. Boots, and C.-A. Cheng, "Safe reinforcement learning using advantage-based intervention," in *International Conference on Machine Learning*. PMLR, 2021, pp. 10 630–10 640.
- [24] L. Zhang, Q. Zhang, L. Shen, B. Yuan, and X. Wang, "Saferl-kit: Evaluating efficient reinforcement learning methods for safe autonomous driving," *arXiv preprint arXiv:2206.08528*, 2022.
- [25] R. S. Sutton and A. G. Barto, *Reinforcement learning: An introduction*. MIT press, 2018.
- [26] E. Squires, R. Konda, S. Coogan, and M. Egerstedt, "Model free barrier functions via implicit evading maneuvers," *arXiv preprint arXiv:2107.12871*, 2021.
- [27] J. Tang, N. Xie, K. Li, Y. Liang, and X. Shen, "Trajectory tracking control for fixed-wing uav based on ddpg," *Journal of Aerospace Engineering*, vol. 37, no. 3, p. 04024012, 2024.
- [28] T. G. Molnar, S. K. Kannan, J. Cunningham, K. Dunlap, K. L. Hobbs, and A. D. Ames, "Collision avoidance and geofencing for fixed-wing aircraft with control barrier functions," *arXiv preprint arXiv:2403.02508*, 2024.
- [29] J. D. Boskovic, L. Chen, and R. K. Mehra, "Adaptive control design for nonaffine models arising in flight control," *Journal of guidance, control, and dynamics*, vol. 27, no. 2, pp. 209–217, 2004.
- [30] P. Glotfelter, J. Cortés, and M. Egerstedt, "Nonsmooth barrier functions with applications to multi-robot systems," *IEEE control systems letters*, vol. 1, no. 2, pp. 310–315, 2017.
- [31] L. Wang, A. D. Ames, and M. Egerstedt, "Multi-objective compositions for collision-free connectivity maintenance in teams of mobile robots," in *2016 IEEE 55th Conference on Decision and Control (CDC)*. IEEE, 2016, pp. 2659–2664.
- [32] U. Bormann, L. Wang, A. D. Ames, and M. Egerstedt, "Control barrier certificates for safe swarm behavior," *IFAC-PapersOnLine*, vol. 48, no. 27, pp. 68–73, 2015.
- [33] E. G. Squires, "Barrier functions and model free safety with applications to fixed wing collision avoidance," Ph.D. dissertation, Georgia Institute of Technology, 2021.
- [34] L. Wang, A. D. Ames, and M. Egerstedt, "Safe certificate-based maneuvers for teams of quadrotors using differential flatness," in *2017 IEEE International Conference on Robotics and Automation (ICRA)*. IEEE, 2017, pp. 3293–3298.
- [35] P. Polack, F. Alché, B. d'Andréa Novel, and A. de La Fortelle, "The kinematic bicycle model: A consistent model for planning feasible trajectories for autonomous vehicles?" in *2017 IEEE intelligent vehicles symposium (IV)*. IEEE, 2017, pp. 812–818.
- [36] W. Zhao, Y. Sun, F. Li, R. Chen, R. Liu, T. Wei, and C. Liu, "GUARD: A safe reinforcement learning benchmark," *Transactions on Machine Learning Research*, 2024. [Online]. Available: <https://openreview.net/forum?id=kZFKwApeQO>
- [37] J. Schulman, S. Levine, P. Abbeel, M. Jordan, and P. Moritz, "Trust region policy optimization," in *International conference on machine learning*. PMLR, 2015, pp. 1889–1897.
- [38] M. El Adawy, E. H. Abdelhalim, M. Mahmoud, I. H. Mohamed, M. M. Othman, G. S. ElGamal, Y. H. ElShabasy *et al.*, "Design and fabrication of a fixed-wing unmanned aerial vehicle (uav)," *Ain Shams Engineering Journal*, vol. 14, no. 9, p. 102094, 2023.
- [39] S. Boyd and L. Vandenberghe, *Convex optimization*. Cambridge university press, 2004.
- [40] T. Haarnoja, A. Zhou, K. Hartikainen, G. Tucker, S. Ha, J. Tan, V. Kumar, H. Zhu, A. Gupta, P. Abbeel *et al.*, "Soft actor-critic algorithms and applications," *arXiv preprint arXiv:1812.05905*, 2018.
- [41] J. Foerster, N. Nardelli, G. Farquhar, T. Afouras, P. H. Torr, P. Kohli, and S. Whetton, "Stabilising experience replay for deep multi-agent reinforcement learning," in *International conference on machine learning*. PMLR, 2017, pp. 1146–1155.
- [42] S. Mehrotra, C. Deguchi, O. Vereschak, C. M. Jonker, and M. L. Tielman, "A systematic review on fostering appropriate trust in human-ai interaction: Trends, opportunities and challenges," *ACM Journal on Responsible Computing*, vol. 1, no. 4, pp. 1–45, 2024.